Cobalt Catalysts

International Edition: DOI: 10.1002/anie.201504707
German Edition: DOI: 10.1002/ange.201504707

Coordination Chemistry of [Co(acac)$_2$] with N-Doped Graphene: Implications for Oxygen Reduction Reaction Reactivity of Organometallic Co-O$_4$-N Species

Jongwoo Han, Young Jin Sa, Yeonjun Shim, Min Choi, Noejung Park, Sang Hoon Joo, and Sungjin Park**

Abstract: *Hybridization of organometallic complexes with graphene-based materials can give rise to enhanced catalytic performance. Understanding the chemical structures within hybrid materials is of primary importance. In this work, archetypical hybrid materials are synthesized by the reaction of an organometallic complex, [Co^{II}(acac)$_2$] (acac = acetylacetonate), with N-doped graphene-based materials at room temperature. Experimental characterization of the hybrid materials and theoretical calculations reveal that the organometallic cobalt-containing species is coordinated to heterocyclic groups in N-doped graphene as well as to its parental acac ligands. The hybrid material shows high electrocatalytic activity for the oxygen reduction reaction (ORR) in alkaline media, and superior durability and methanol tolerance to a Pt/C catalyst. Based on the chemical structures and ORR experiments, the catalytically active species is identified as a Co-O$_4$-N structure.*

Transition-metal-based organometallic compounds are an important class of molecular catalysts in various applications owing to their highly tunable properties, such as coordination numbers, oxidation states of metal centers, and binding structures between metals and ligands.[1] Their catalytic performances can be tuned by modulating electronic, chemical, and steric interactions between the metal atoms and surrounding organic ligands. Recently, it was reported that coordination of carbon-based nanomaterials, such as chemically modified graphenes (CMGs), carbon nanotubes, and carbon nitride, to organometallic molecules can dramatically change catalytic performances.[2–5] Since carbon-based nanomaterials can have fast electron transfer throughout the carbon network and good tolerance for chemical modification, the formation of new hybrid systems containing molecular entities attached to carbon-based nanomaterials may be advantageous in electrocatalytic reactions, which require fast electron transfer and facile access of reactants to active sites. Carbon-based nanomaterials doped with transition metals (Co and/or Fe) and nitrogen atoms (M-N-C catalysts) have been of particular attention as electrocatalysts for the oxygen reduction reaction (ORR), as they can potentially replace Pt-based catalysts that are costly and scarce.[6–10] The preparation of highly active M-N-C catalysts in most cases requires a high-temperature heating step under reactive gas. Yet, from a fundamental point of view, such high-temperature treatments render the identification of catalytically active structures elusive, resulting in the catalyst preparation being far from rational, predictive, and cost-effective.

Herein, the rational synthesis at room temperature of archetypical hybrid materials consisting of cobalt-based organometallic complexes ([Co(acac)$_2$], acac = acetylacetonate) coordinated to N-doped graphenes is reported (Figure 1 a). The coordination nature in the hybrid materials was comprehensively dissected by using solid-state nuclear magnetic resonance (SSNMR) with isotope labeling, X-ray photoelectron spectroscopy (XPS), X-ray absorption spectroscopy, and density functional theory (DFT) calculations, which consistently revealed that the Co species was coordinated to the heterocyclic groups in N-doped graphene as well as to its parental acac ligands. The hybrid materials demonstrated excellent performance as electrocatalysts for the ORR. The molecular-level understanding of the chemical structure of the hybrid, as well as the control ORR experiments, enabled the identification of a new type of catalytically active species, Co-O$_4$-N.

Because N-doped CMGs have shown good catalytic performances for ORR, we prepared an N-doped CMG, ammonium hydroxide-reduced graphene oxide (A-rG-O; Supporting Information, Figure S1). Following the precedent of using SSNMR to understand the chemical structures of CMGs,[11,12] we next conducted a magic angle spinning (MAS) SSNMR study of ^{15}N-labeled A-rG-O materials to elucidate the chemical identity of the N components. ^{15}N-labeled ammonium hydroxide was used to prepare ^{15}N-labeled A-rG-O (^{15}N-A-rG-O). The ^{13}C SSNMR spectrum of ^{15}N-A-rG-O showed a significant decrease of peak intensity corresponding to oxygen-containing functional groups relative to G-O indicating successful reduction (Figure 1 b; Supporting

[*] J. Han, Y. Shim, Prof. Dr. S. Park
Department of Chemistry and Chemical Engineering, Inha University
100 Inha-ro, Nam-gu, Incheon 402-751 (Republic of Korea)
E-mail: sungjinpark@inha.ac.kr
Y. J. Sa, Prof. Dr. S. H. Joo
Department of Chemistry,
Ulsan National Institute of Science and Technology (UNIST)
50 UNIST-gil, Ulsan 689-798 (Republic of Korea)
E-mail: shjoo@unist.ac.kr
Prof. Dr. S. H. Joo
School of Energy and Chemical Engineering, UNIST
50 UNIST-gil, Ulsan 689-798 (Republic of Korea)
M. Choi, Prof. Dr. N. Park
Department of Physics and
Center for Multidimensional Carbon Materials, UNIST
50 UNIST-gil, Ulsan 689-798 (Republic of Korea)

Supporting information for this article is available on the WWW under http://dx.doi.org/10.1002/anie.201504707.

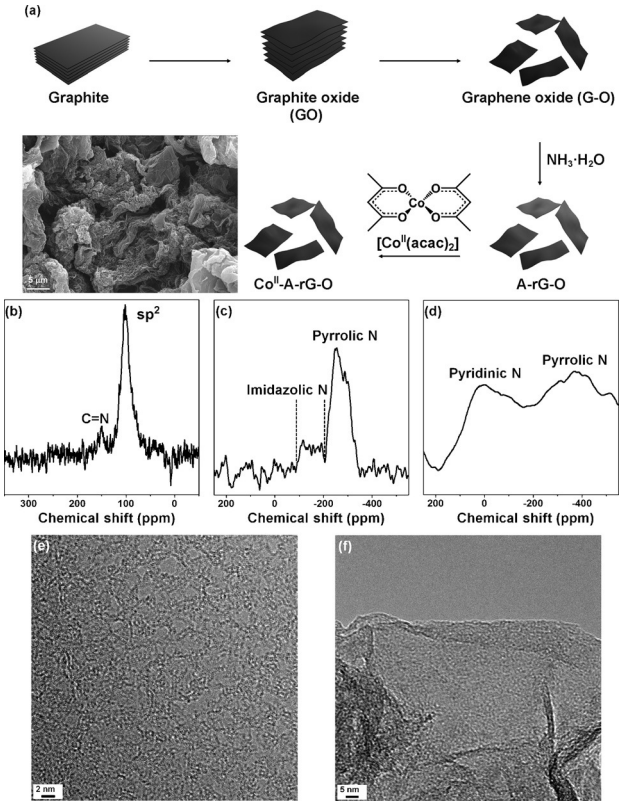

Figure 1. a) Overall approach to produce Co^{II}-A-rG-O materials (inset: an SEM image of Co^{II}-A-rG-O). b) ^{13}C MAS SSNMR spectrum. c) ^{15}N CPMAS SSNMR spectrum. d) ^{15}N MAS SSNMR spectrum of ^{15}N-A-rG-O. e) Cs-corrected TEM image. Scale bar: 2 nm. f) HR TEM image of Co^{II}-A-rG-O. Scale bar: 5 nm.

Information, Figure S2).[11] Importantly, a new peak at 150 ppm, which was not found in the SSNMR spectrum of G-O, appeared in the spectrum of ^{15}N-A-rG-O (Figure 1b). This peak is assigned to the carbon atoms of C=N moieties, suggesting successful incorporation of N atoms into the sp^2 carbon network.[11]

An ^{15}N cross-polarization (CP) MAS SSNMR spectrum of ^{15}N-A-rG-O showed distinct peaks at −250 and −150 ppm, corresponding to pyrrolic and imidazolic groups containing isolated N atoms, respectively (Figure 1c).[13,14] An ^{15}N MAS SSNMR spectrum of ^{15}N-A-rG-O without CP technique showed broad peaks between 200–400 ppm and at about 0 ppm, corresponding to pyrrolic and pyridinic groups, respectively (Figure 1d; Supporting Information, Figures S3–S6).[13,14]

A hybrid material (Co^{II}-A-rG-O) was obtained as black powders by the reaction of A-rG-O with $[Co^{II}(acac)_2]$ at room temperature (Figure 1a; Supporting Information, Figure S7). Co components (2.0 at%; Supporting Information, Table S1) in Co^{II}-A-rG-O were found in XPS measurements. Although many graphene-based hybrid systems require high temperatures for their production, our process could be achieved at low temperature (room temperature), which will be highly beneficial for low cost industrial applications. Previous work has shown that transition-metal compounds often generate inorganic nanoparticles such as metal oxides upon reaction with graphene-based materials.[15,16] Surprisingly, no nanoparticles were found in numerous transmission electron microscopy (TEM) measurements of Co^{II}-A-rG-O samples using high resolution-TEM (HR-TEM) and Cs-corrected TEM instruments, suggesting that Co species are molecularly attached to the surface of A-rG-O materials (Figure 1e,f; Supporting Information, Figure S8).

To understand the chemical environment of Co^{II}-A-rG-O, we prepared a Co^{II}-^{15}N-A-rG-O sample by reaction of $[Co^{II}(acac)_2]$ with ^{15}N-A-rG-O. The ^{13}C MAS SSNMR spectrum of ^{15}N-A-rG-O exhibited no peaks assignable to primary alkyl groups at 0 ppm.[17] On the other hand, a new peak appeared about 0 ppm in the spectrum of the Co^{II}-^{15}N-A-rG-O sample (Figure 2a). It is reasonable to assume that this peak originates from the methyl groups in $[Co^{II}(acac)_2]$

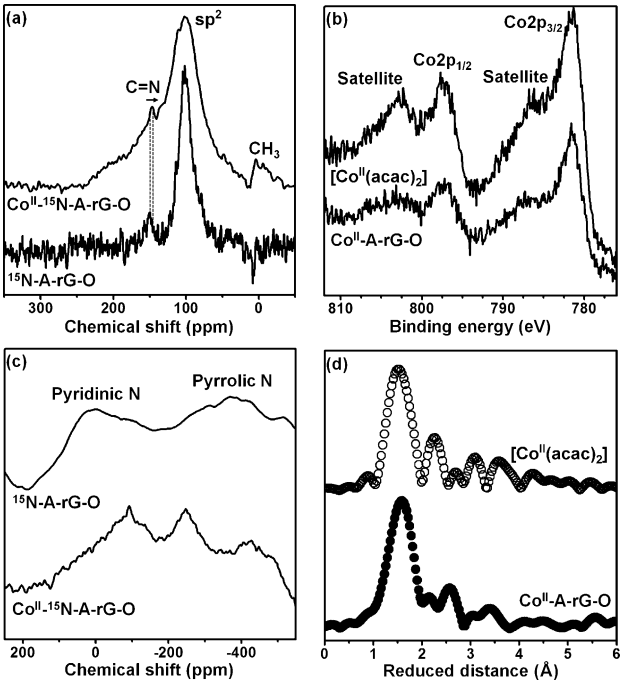

Figure 2. a) ^{13}C MAS SSNMR spectra of ^{15}N-A-rG-O and Co^{II}-^{15}N-A-rG-O. b) XPS Co 2p spectra of $[Co(acac)_2]$ and Co^{II}-A-rG-O. c) ^{15}N MAS SSNMR spectra of ^{15}N-A-rG-O and Co^{II}-^{15}N-A-rG-O. d) Fourier-transformed k^3-weighted EXAFS spectra of $[Co(acac)_2]$ and Co^{II}-A-rG-O.

suggesting that the acac ligands were preserved in the Co^{II}-N-A-rG-O sample after reaction (Supporting Information, Figures S9–S15). The XPS Co 2p spectrum of Co^{II}-A-rG-O showed peaks at 781.6 eV (for Co $2p_{3/2}$) and 797.2 eV (for Co $2p_{1/2}$), which are consistent with the Co^{II} peaks of $[Co^{II}(acac)_2]$ (Figure 2b). Furthermore, each peak exhibited satellites, which is evidence that the oxidation state of the Co atoms in Co^{II}-A-rG-O is +2.[18] The Co 3p XPS spectra of $[Co^{II}(acac)_2]$ and Co^{II}-A-rG-O were similar to each other, showing a peak at 62 eV, which corresponds to Co−O bonds (Supporting Information, Figure S14).[19] These data suggest that the oxidation state of Co is +2 and that the acac ligands of $[Co^{II}(acac)_2]$ remain coordinated to the metal after forming the Co^{II}-A-rG-O hybrid material (Supporting Information).

Another notable feature in the ^{13}C MAS SSNMR spectrum of Co^{II}-^{15}N-A-rG-O was the significant broadening of the peak corresponding to sp^2 carbons around 100 ppm relative to that of ^{15}N-A-rG-O sample (Figure 2a). Chemical binding between some sp^2 carbons and organometallic molecules could be responsible for this broadening. Furthermore, the ^{13}C SSNMR peak corresponding to C=N moieties was shifted slightly from 150 to 146 ppm after attachment of the Co species. This suggests the presence of a chemical interaction between the N-containing aromatic rings in A-rG-O and Co. After reaction with $[Co^{II}(acac)_2]$ peaks at −400, −250, and −100 ppm were observed in the ^{15}N MAS SSNMR spectrum of Co^{II}-^{15}N-A-rG-O (Figure 2c). The peaks at −400 and −100 ppm were assigned to pyrrolic and pyridinic N, respectively, and are shifted to lower ppm than the corresponding signals in A-rG-O. These shifts are consistent with coordination of these heterocyclic nitrogen groups to Co-based species.

The local environment surrounding the incorporated cobalt atoms was further investigated by X-ray absorption near edge structure (XANES) and extended X-ray absorption fine structure (EXAFS). The XANES spectrum of Co^{II}-A-rG-O indicated that Co atoms have distorted octahedral or five-coordinate square pyramidal structure (Supporting Information, Figure S16). The Fourier-transformed radial distribution functions (RDFs) for EXAFS spectra (Figure 2d) revealed a clear difference between Co^{II}-A-rG-O and $[Co^{II}(acac)_2]$. For a primary peak observed at 1.5–1.6 Å, the distance for Co^{II}-A-rG-O (1.59 Å) was slightly longer than that for $[Co^{II}(acac)_2]$ (1.52 Å).[20] The positions of the next two peaks were also observed at longer distances for the Co^{II}-A-rG-O than for $[Co^{II}(acac)_2]$ (Supporting Information). These observations indicated that the bond distances between Co and adjacent O and C atoms in the Co^{II}-A-rG-O are elongated compared to those with $[Co^{II}(acac)_2]$.

We performed the first-principle DFT calculations for the purpose of identifying stable binding mechanism of $[Co^{II}(acac)_2]$ to possible binding sites including N-containing aromatic rings (Supporting Information, Figures S17, S18). Our calculations of all possible binding modes suggests that chemisorption of $[Co^{II}(acac)_2]$ on the surface of CMGs is energetically favorable. The pyridine-type structure has the strongest binding affinity for $[Co^{II}(acac)_2]$ (Supporting Information, Figure S18). The main binding mechanism is due to partial charge transfer from $[Co^{II}(acac)_2]$ to the aromatic structure of the CMG materials indicating that the CMG can withdraw electrons from $[Co^{II}(acac)_2]$. This electron transfer can consequently weaken the bonding strength between Co and parental acac ligands, which can corroborate the bond elongation phenomena observed with the Co^{II}-A-rG-O revealed by the above EXAFS results. Overall, the SSNMR, XPS, EXAFS, and DFT calculation results consistently suggest that N-containing heterocyclic groups in A-rG-O are coordinated to Co^{II}-containing molecules.

We next explored the electrocatalytic activity of hybrid samples for the ORR. The Co^{II}-A-rG-O showed much more positively shifted linear sweep voltammetry (LSV) curve than A-rG-O, indicating enhanced ORR activity by the attachment of $[Co^{II}(acac)_2]$ (Figure 3a). Co^{II}-A-rG-O exhibited onset and

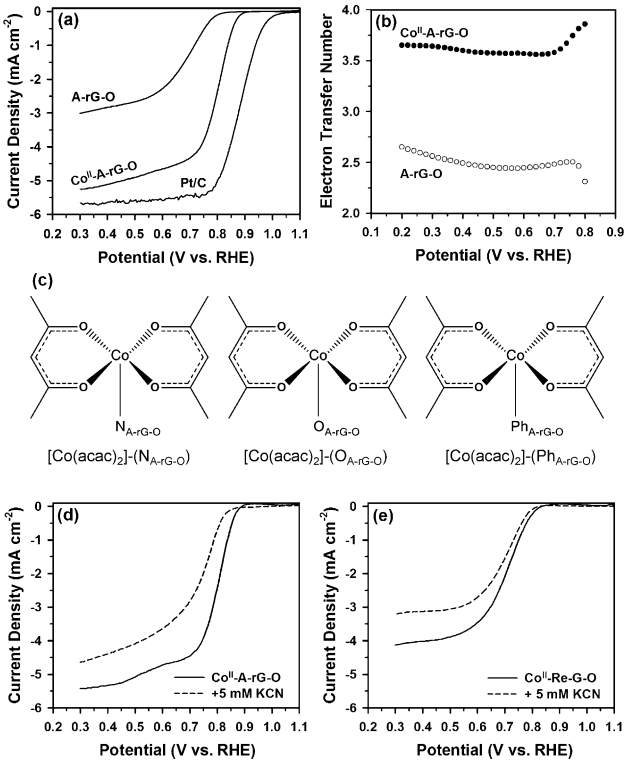

Figure 3. a) LSV curves of A-rG-O, Co^{II}-A-rG-O, and Pt/C catalysts for the ORR. b) Electron transfer number of A-rG-O and Co^{II}-A-rG-O. c) Possible active species of Co^{II}-A-rG-O for the ORR. d) LSV curves of Co^{II}-A-rG-O. e) Co^{II}-Re-G-O in the presence and absence of 5 mM KCN.

half-wave potentials at 0.88 V and 0.81 V, respectively, which are close to those of the commercial Pt/C catalyst (ca. 1.0 V and 0.88 V). Kinetic current density at 0.8 V for Co^{II}-A-rG-O was 8.9 mA cm^{-2}, which is 88 times higher than that A-rG-O. The hybrid also exhibited better ORR kinetics than A-rG-O, as revealed by four-electron selectivity and Tafel slopes (Figure 3b; Supporting Information, Figure S19). These results suggest that interactions between $[Co^{II}(acac)_2]$ and A-rG-O create highly efficient active sites for the ORR, which leads to enhanced kinetics and ORR activity for Co^{II}-A-rG-O. The half-wave potential and 4-electron selectivity of previously reported, highly active Co-N-C catalysts revealed that our Co^{II}-A-rG-O compared favorably with the most active Co-N-C catalysts (Supporting Information, Table S2). The preparation of Co-N-C catalysts displaying high catalytic activity typically requires high temperature and/or pressure, as well as the use of strong reductants.[21–27] It is noteworthy that our high performance ORR catalysts were prepared by simple mixing of organometallic complexes and N-doped CMG materials at room temperature. The Co^{II}-A-rG-O also showed very high stability (Supporting Information, Figure S20). After 10000 cycles between 0.6 and 1.0 V (vs. RHE), the ORR activity of the Co^{II}-A-rG-O decreased minimally, with a negative shift of only 11 mV in the half-wave potential. Furthermore, the Co^{II}-A-rG-O showed excellent poison-tolerance as revealed by an almost identical LSV curve after the addition of methanol.

To clarify the role of nitrogen in the enhancement of ORR activity, we prepared another graphene-based sample (refluxed graphene oxide, Re-G-O; Supporting Information, Figures S21–S25), which contains a similar C/O ratio (5.0) to A-rG-O (5.7), but no N atom. We measured the ORR activity and four-electron transfer selectivity of Re-G-O and [Co^{II}-$(acac)_2$]-attached Re-G-O (Co^{II}-Re-G-O), and compared with those of Co^{II}-A-rG-O (Supporting Information, Figure S26). Co^{II}-Re-G-O exhibited a much lower ORR activity than Co^{II}-A-rG-O, as evidenced by lower onset potential (around 90 mV) and four-electron selectivity. The main difference between the Co^{II}-Re-G-O and Co^{II}-A-rG-O samples was the presence of N-related sites in Co^{II}-A-rG-O. Therefore, the possibility is ruled out that the high onset potential of Co^{II}-A-rG-O can be attributed to [$Co(acac)_2$]–($O_{A\text{-}rG\text{-}O}$) and/or [$Co(acac)_2$](phenyl group (Ph)$_{A\text{-}rG\text{-}O}$) sites (Figure 3c). This claim can be substantiated by comparing the LSV curves of Co^{II}-Re-G-O and Re-G-O (Supporting Information, Figure S26). These two samples showed almost the same onset potential, but Co^{II}-Re-G-O showed a greater diffusion current density than Re-G-O. This indicates that the presence of [$Co(acac)_2$]–($O_{Re\text{-}G\text{-}O}$) and [$Co(acac)_2$]–($Ph_{Re\text{-}G\text{-}O}$) sites in Co^{II}-Re-G-O has only a marginal promotional effect in ORR activity. These results highlight the importance of formation of additional binding between a Co-O_4 cluster and an N-containing species in A-rG-O to generate a Co-O_4-N species that is active for the ORR.

To further analyze the nature of the proposed active sites, a poisoning test with potassium cyanide (KCN) was performed. In the presence of 5 mM KCN in 0.1M KOH a roughly 50 mV decrease in onset potential was observed for Co^{II}-A-rG-O (Figure 3d). However, no shift in onset potential was observed for Co^{II}-Re-G-O in the poisoning test (Figure 3e). In both catalysts, the cobalt centers were blocked by CN^- ions, as evidenced by the decreased current densities. The poisoning experiments and the above characterizations lead to the conclusion that the [$Co(acac)_2$]–($N_{A\text{-}rG\text{-}O}$) cluster in Co-A-rG-O is the major active site for a more positive ORR onset potential and greater four-electron selectivity, while [$Co(acac)_2$]–($O_{A\text{-}rG\text{-}O}$) and [$Co(acac)_2$]–($Ph_{A\text{-}rG\text{-}O}$) play an auxiliary role through disproportionation and/or reduction of HO_2^-, a reaction intermediate.

Taking all evidences into account, we suggest a new type of ORR active site in alkaline media: a Co atom coordinated to two acac ligands in a square planar arrangement, and an additional N atom (or N-containing aromatic ring) at an axial position (Figure 3c). The proposed active site differs from the Co-N_2 and Co-N_4 sites in typical pyrolyzed Co-N-C catalysts in that there is only a single coordinating nitrogen. Interestingly, an analogous local structure can be found in the natural ORR-catalyzing center of cytochrome *c* oxidase (CcO), where an Fe atom binds to four heme nitrogen atoms and an axial imidazolic N forming a five-coordinate square-pyramidal structure.[28] Further detailed investigations are underway for dissecting the structure and reactivity of Co-O_x-N_y type active sites.

In conclusion, we synthesized novel hybrid materials by coordinating [$Co^{II}(acac)_2$] to N-doped A-rG-O using a solution process at room temperature. ^{13}C and ^{15}N SSNMR measurements using isotope labeling, XANES/EXAFS, and DFT calculations revealed that the N-containing groups in A-rG-O coordinate to a Co^{II} atom having two chelating acac ligands in square planar positions and N at an axial position. The hybrids show excellent electrocatalytic activity towards O_2 reduction in alkaline media, and superior durability and MeOH tolerance in the ORR. Combining the molecular-level structural understanding and control ORR experiments allows for the identification of a catalytically active species, Co-O_4-N. Our room temperature coordination between organometallic molecules and graphene-based materials ensures the preservation of precursor structures, which allows greater predictability of local structure around the metal center. Ultimately, our approach would enable the design of novel electrocatalysts in a more rational fashion.

Acknowledgements

S.P. thanks the Korea Basic Science Institute (KBSI) for the XPS and SSNMR analysis. The XANES/EXAFS experiments performed at the beamline 10C of Pohang Accelerator Laboratory (PAL) were supported in part by the Ministry of Education and POSTECH. J.H., Y.S., and S.P. were supported by a grant from the Center for Advanced Soft Electronics funded by the Ministry of Science, ICT & Future Planning as a Global Frontier Project (CASE-2014M3A6A5060938). S.H.J. was supported by the Basic Science Research Program through the National Research Foundation (NRF) of Korea (NRF-2013R1A1A2012960). Y.J.S. acknowledges the Global Ph.D. Fellowship (NRF-2013H1A2A1032644). N.P. and M.C. were supported by the Basic Science Research Program through the National Research Foundation of Korea funded by the Ministry of Education (NRF-2013R1A1A2007910).

Keywords: cobalt · electrocatalysis · heterogeneous catalysis · nanomaterials · solid-state NMR

How to cite: *Angew. Chem. Int. Ed.* **2015**, *54*, 12622–12626
Angew. Chem. **2015**, *127*, 12813–12817

[1] G. L. Miessler, P. J. Fisher, D. A. Tarr, *Inorganic Chemistry*, 5th ed., Prentice Hall, New Jersey, **2013**.
[2] V. C. Gibson, S. K. Spitzmesser, *Chem. Rev.* **2003**, *103*, 283–316.
[3] L. Resconi, L. Cavallo, A. Fait, F. Piemontesi, *Chem. Rev.* **2000**, *100*, 1253–1346.
[4] B. Choi, J. Lee, S. Lee, J. Ko, K. Lee, J. Oh, J. Han, Y. Kim, I. S. Choi, S. Park, *Macromol. Rapid Commun.* **2013**, *34*, 533–538.
[5] R. Kuriki, K. Sekizawa, O. Ishitani, K. Maeda, *Angew. Chem. Int. Ed.* **2015**, *54*, 2406–2409; *Angew. Chem.* **2015**, *127*, 2436–2439.
[6] R. Bashyam, P. Zelenay, *Nature* **2006**, *443*, 63–66.
[7] M. Lefèvre, E. Proietti, F. Jaouen, J. Dodelet, *Science* **2009**, *324*, 71–74.
[8] G. Wu, K. L. More, C. M. Johnston, P. Zelenay, *Science* **2011**, *332*, 443–447.
[9] K. Parvez, S. Yang, Y. Hernandez, A. Winter, A. Turchanin, X. Feng, K. Müllen, *ACS Nano* **2012**, *6*, 9541–9550.
[10] J. Y. Cheon, T. Kim, Y. Choi, H. Y. Jeong, M. G. Kim, Y. J. Sa, J. Kim, Z. Lee, T. Yang, K. Kwon, O. Terasaki, G. Park, R. R. Adzic, S. H. Joo, *Sci. Rep.* **2013**, *3*, 2715.

[11] S. Park, Y. Hu, J. O. Hwang, E. Lee, L. B. Casabianca, W. Cai, J. R. Potts, H. Ha, S. Chen, J. Oh, *Nat. Commun.* **2012**, *3*, 638.
[12] G. Park, S. K. Park, J. Han, T. Y. Ko, S. Lee, J. Oh, S. Ryu, H. S. Park, S. Park, *RSC Adv.* **2014**, *4*, 36377 – 36384.
[13] N. Baccile, G. Laurent, C. Coelho, F. Babonneau, L. Zhao, M. Titirici, *J. Phys. Chem. C* **2011**, *115*, 8976 – 8982.
[14] M. S. Solum, K. L. Altmann, M. Strohmeier, D. A. Berges, Y. Zhang, J. C. Facelli, R. J. Pugmire, D. M. Grant, *J. Am. Chem. Soc.* **1997**, *119*, 9804 – 9809.
[15] S. Lee, J. Y. Cheon, W. J. Lee, S. O. Kim, S. H. Joo, S. Park, *Carbon* **2014**, *80*, 127 – 134.
[16] Y. Liang, Y. Li, H. Wang, J. Zhou, J. Wang, T. Regier, H. Dai, *Nat. Mater.* **2011**, *10*, 780 – 786.
[17] P. Adriaensens, L. Storme, R. Carleer, J. Gelan, F. Du Prez, *Macromolecules* **2002**, *35*, 3965 – 3970.
[18] M. Domínguez, E. Taboada, H. Idriss, E. Molins, J. Llorca, *J. Mater. Chem.* **2010**, *20*, 4875 – 4883.
[19] R. Dedryvère, S. Laruelle, S. Grugeon, P. Poizot, D. Gonbeau, J. Tarascon, *Chem. Mater.* **2004**, *16*, 1056 – 1061.
[20] P. O'Day, J. Rehr, S. Zabinsky, G. J. Brown, *J. Am. Chem. Soc.* **1994**, *116*, 2938 – 2949.
[21] Q. Liu, J. Zhang, *Langmuir* **2013**, *29*, 3821 – 3828.
[22] Z. Liu, G. Zhang, Z. Lu, X. Jin, Z. Chang, X. Sun, *Nano Res.* **2013**, *6*, 293 – 301.
[23] Z. Wu, L. Chen, J. Liu, K. Parvez, H. Liang, J. Shu, H. Sachdev, R. Graf, X. Feng, K. Müllen, *Adv. Mater.* **2014**, *26*, 1450 – 1455.
[24] K. Asazawa, H. Kishi, H. Tanaka, D. Matsumura, K. Tamura, Y. Nishihata, A. G. Saputro, H. Nakanishi, H. Kasai, K. Artyushkova, *J. Phys. Chem. C* **2014**, *118*, 25480 – 25486.
[25] T. S. Olson, S. Pylypenko, P. Atanassov, K. Asazawa, K. Yamada, H. Tanaka, *J. Phys. Chem. C* **2010**, *114*, 5049 – 5059.
[26] D. Shin, B. Jeong, B. S. Mun, H. Jeon, H. Shin, J. Baik, J. Lee, *J. Phys. Chem. C* **2013**, *117*, 11619 – 11624.
[27] S. Jiang, C. Zhu, S. Dong, *J. Mater. Chem. A* **2013**, *1*, 3593 – 3599.
[28] J. P. Collman, N. K. Devaraj, R. A. Decreau, Y. Yang, Y. L. Yan, W. Ebina, T. A. Eberspacher, C. E. Chidsey, *Science* **2007**, *315*, 1565 – 1568.

Received: May 25, 2015
Revised: July 25, 2015
Published online: September 2, 2015

